Int. J. Electrochem. Sci., 6 **(2011)** 1642 - 1654

International Journal of
ELECTROCHEMICAL
SCIENCE
www.electrochemsci.org

Platinum Particles Embedded into Nanowires of Polyaniline Doped With Poly(Acrylic Acid-co-Maleic Acid) as Electrocatalyst for Methanol Oxidation

Chang-Cian Yang[1], *Tzi-yi Wu*[2,3], *Ho-Rei Chen*[1], *Tar-Hwa Hsieh*[1], *Ko-Shan Ho*[1], *Chung-Wen Kuo*[1,*]

[1]Department of Chemical and Materials Engineering, National Kaohsiung University of Applied Sciences, Kaohsiung 807, Taiwan
[2]Department of Chemistry, National Cheng Kung University, Tainan 70101, Taiwan
[3]Department of Materials Engineering, Kun Shan University, Tainan 71003, Taiwan
[*]E-mail: welly@cc.kuas.edu.tw

Received: 15 March 2011 / *Accepted:* 6 April 2011 / *Published:* 1 May 2011

Polyaniline-poly(acrylic acid-co-maleic acid) (PANI-PAMA) with a nanowire network structure is prepared using a doping-dedoping-redoping route. Platinum (Pt) particles are deposited into PANI and PANI-PAMA nanowire network structures via a potentiostatic process to obtain PANI-Pt and PANI-PAMA-Pt composite electrodes, respectively. Functional group analysis is conducted using Fourier transform infrared (FT-IR) spectroscopy and the morphology of PANI-PAMA is determined using scanning electron microscopy (SEM). SEM images reveal that PANI-PAMA is composed of highly porous nanowires. The structures of PANI-Pt and PANI-PAMA-Pt composite electrodes are further characterized using X-ray photoelectron spectroscopy (XPS), electron dispersive element analysis (EDS), and Auger electron spectroscopy (AES). The EDS and AES results indicate that the Pt is dispersed uniformly in the PANI-PAMA matrix. The cyclic voltammetry (CV) results and chronopotentiometry measurements demonstrate that the electrocatalytic activity and stability for methanol oxidation of the PANI-PAMA-Pt composite are higher than those of PANI-Pt.

Keywords: polyaniline, poly(acrylic acid-co-maleic acid), nanowire, cyclic voltammetry, AES, methanol oxidation

1. INTRODUCTION

Direct methanol fuel cells (DMFCs) are promising power sources for various applications due to their low operating temperatures, relatively quick start-up, and the high theoretical power density of liquid methanol fuel [1-9]. However, important problems must be still solved to make DMFCs

commercially viable, such as the relatively poor kinetics of the methanol oxidation on the anode, generally a Pt-based catalyst, and the self-poisoning of the Pt catalyst by $(CO)_{ad}$, an intermediate product of the methanol oxidation [10,11]. To overcome these problems, researchers have utilized catalysts with a high surface area [12,13]. The supporting materials for the dispersion of Pt particles play an important role in methanol oxidation [14].

Conducting polymers are considered interesting supporting materials for catalyst particles. It has been shown that electrodes modified with a polymer exhibit better catalytic performance for methanol oxidation than those without a polymer. The high surface area of conducting polymers makes them suitable as supporting materials for the development of new electrocatalysts [15,16]. Li and Lin [17] deposited Pt nanoclusters into polypyrrole (PPy) nanowires using the cyclic voltammetry method. The 3D PPy-Pt composite exhibited higher electrocatalytic activity toward methanol oxidation reactions than did a pure Pt-modified glass carbon electrode. Liu *et al.* [18] prepared polyaniline nanowire structures via a galvanostatic process. The PANI-Pt nanocomposite electrode exhibited excellent catalytic activity for methanol oxidation in comparison to that of a bulk Pt electrode. Xie *et al.* [19] fabricated a 3D electrode using PPy-coated polystyrene spheres covered by a platinum catalyst. The electrode exhibited superior properties for methanol oxidation compared to those of a conventionally prepared electrode. Chang *et al.* [20] synthesized a stable film of poly(2,5-dimethoxyaniline-co-2,5-diaminobenzenesulphonic acid) using electrochemical deposition. The existence of a $-SO_3H$ group in the copolymer might help the electrodeposition of Pt. These results show that Pt particles embedded into a conducting polymer lead to good catalytic activity for methanol oxidation.

Recently, a polymer acid, poly(styrenesulfonic acid) (PSS), has been shown to be easily incorporated in a conducting polymer matrix as a dopant as support for Pt particles. Huang *et al.* [21] reported that PANI-PSS acts as a matrix for the uniform distribution of Pt particles. As a result, the electrocatalytic activity for methanol oxidation of PANI-PSS-Pt is much higher than that of PANI-Pt. Kuo *et al.* [22] reported that highly dispersed Pt particles homogeneously distributed into a poly(3,4-ethylenedioxythiophene)-poly(styrene sulfonic acid) (PEDOT-PSS) matrix. However, these investigations mainly focused on the manufacture of PSS as a dopant in a conducting polymer matrix; less attention has been given to the processing of a conducting polymer modified with a polymer acid containing carboxylic acid for supporting materials of direct methanol fuel cells. Wang *et al.* [23] reported that Ag nanoparticles are uniformly distributed in poly(allylamine hydrochloride)/poly(acrylic acid) (PAH/PAA) multilayers and absent from PAH/PSS multilayers. This can be attributed to the weak interaction between PAH and $-CO_2H$ groups of the weak acid PAA, which provides more network pore space with Ag^+ and facilitates the preparation of Ag nanoparticles. This motivated us to investigate the feasibility of incorporating $-CO_2H$ groups into PANI as support for Pt.

In this study, we employed a simple doping-dedoping-redoping method to introduce $-CO_2H$ groups (poly(acrylic acid-co-maleic acid), PAMA) into a PANI matrix. PANI doped with PAMA forms a spatial network structure, which behaves as a 3D-random matrix for the deposition Pt particles. We believe that PANI-PAMA may act as a stabilizer for Pt particles, preventing their aggregation. The PANI-PAMA-Pt composite is expected to enhance electroactivity for methanol oxidation.

2. EXPERIMENTAL

2.1. Preparation of PANI-PAMA

A mixture solution of 0.1 M ANI (Merck) and 0.5 M H_2SO_4 (Merck) aqueous solution was prepared. Electrochemical polymerization of the solution was carried out using the galvanostatic method with ITO as the working electrode for a total charge of 0.1 C/cm^2, as described elsewhere [24]. Before each experiment, indium tin oxide (ITO)-coated glass was cleaned in an ultrasonic bath using detergent, double-distilled water, and isopropanol, and then dried with a dry nitrogen flow, followed by UV-O_3 treatment for 30 min. The electrochemically deposited PANI film was rinsed with double-distilled water for 5 min and then dried at 120 ^oC for 3 min. The emeraldine base (EB) form of PANI was obtained by treating the PANI film in 0.1 M ammonium hydroxide (Aldrich) for 30 min. The EB film was redoped with poly(acrylic acid-co-maleic acid) (PAMA) (M_w = 3,000, Aldrich). PANI doped with PAMA is denoted as PANI-PAMA.

2.2. Deposition of Pt in PANI-PAMA matrix

Pt particles were incorporated into PANI-PAMA film by electrochemical deposition from a solution [0.01 M HCl + 0.1 M KCl solution containing 5 mM $H_2PtCl_6 \cdot 6H_2O$] (PANI-PAMA-Pt) with a constant deposition charge of 0.15 C at a constant potential of -0.2 V (vs. Ag/AgCl). For comparison, Pt particles were also deposited on a PANI matrix (PANI-Pt) using a method similar to that for the deposition of Pt particles onto PANI-PAMA. After Pt particles were incorporated into the matrix, the electrodes were rinsed with double-distilled water for 5 min and then dried at 120 ^oC for 3 min.

2.3. Characterization of PANI-PAMA-Pt composite electrode

The Fourier transform infrared (FT-IR) spectra of PANI-H_2SO_4 (emeraldine salt), emeraldine base (EB), and PANI redoped with PAMA (PANI-PAMA, emeraldine salt) in KBr pellets were obtained using a Perkin Elmer FT-IR instrument with a resolution of 4 cm^{-1}. The average of 16 scans was used to obtain each spectrum. All samples were vacuum-dried overnight prior to measurement. An X-ray photoelectron spectroscopy (XPS) study was performed with ESCA 210 spectrometers. The XPS spectra employed Mg Kα ($h\nu$ = 1253.6 eV) irradiation as the photon source, with a primary tension of 12 kV. The pressure during the scans was approximately 10^{-10} mbar. The surface morphologies of PANI-PAMA-Pt and PANI-Pt films were obtained using scanning electron microscopy (SEM) (JEOL JSM-6700F) and energy dispersive spectroscopy (EDS). Auger electron spectroscopy (AES) depth profiles were obtained with a Microlab 310 D (VG Scientific Ltd.) spectrometer at emission currents of 0.1 and 8 mA with gun tensions of 10 kV (electron) and 3 kV (ion), respectively.

Electrochemical characterizations of PANI-PAMA-Pt and PANI-Pt composite electrodes were carried out using a PGSTAT30 electrochemical analyzer, AUTOLAB Electrochemical Instrument (The Netherlands). All experiments were performed in a three-component cell. An Ag/AgCl electrode

(in 3 M KCl), a Pt wire, and an ITO-coated glass plate (1 cm^2 area) were used as the reference, counter, and working electrodes, respectively. A Luggin capillary, whose tip was set at a distance of 1-2 mm from the surface of the working electrode, was used to minimize errors due to an *iR* drop in the electrolytes. An impedance spectrum analyzer was employed to measure and analyze the AC impedance spectra of electrodes obtained at various element resistance values. For the AC signal, the potential amplitude was kept at 10 mV and the frequency range was 1 mHz to 10 kHz.

2.4. Methanol electrooxidation of PANI-PAMA-Pt composite electrode

The catalytic activities of PANI-PAMA-Pt and PANI-Pt composite electrodes were examined by cyclic voltammetry (CV) at 10 mV/sec in a range of -0.2 to 1.0 V and potential-time curves were obtained at 0.08 mA/cm^2 in 0.1 M CH_3OH + 0.5 M H_2SO_4 solution. All the electrochemical experiments were carried out at room temperature.

3. RESULTS AND DISCUSSION

3.1. FT-IR analysis of PANI and PANI-PAMA

The FT-IR spectra of doped PANI (electrochemical polymerization of PANI in H_2SO_4 medium), dedoped PANI (emeraldine base), and PANI redoped with PAMA are shown in Fig. 1a-c, respectively. The doped PANI (doped with H_2SO_4, curve a) exhibits some peaks. The absorption peak at 801 cm^{-1} is attributed to the para-substituted aromatic out-of-plain bending.

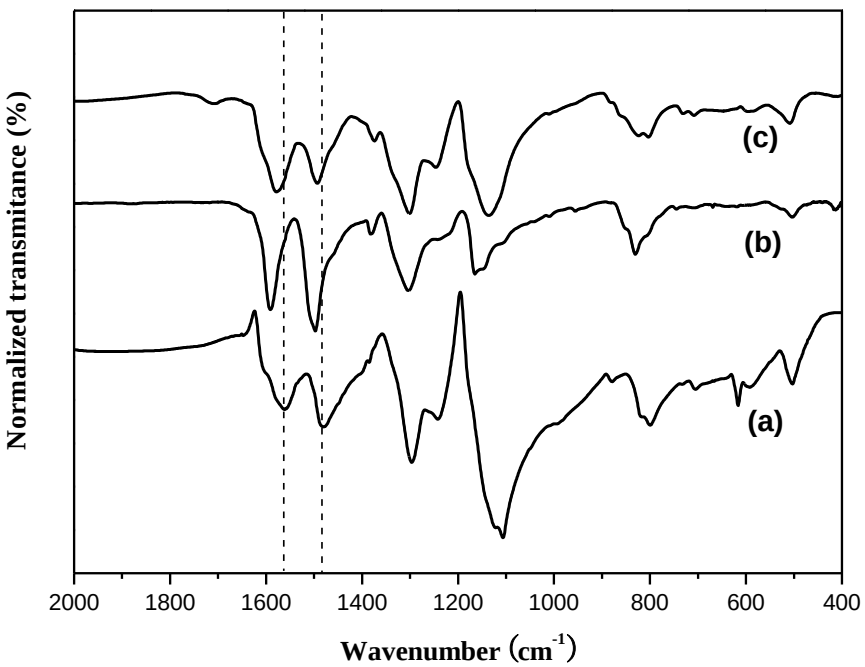

Figure 1. FT-IR spectra of (a) PANI-H_2SO_4 (emeraldine salt), (b) emeraldine-base (EB) PANI, and (c) PANI redoped with PAMA (PANI-PAMA, emeraldine salt).

The absorption peaks of the -S=O group in PANI-H_2SO_4 are located at 1000 and 1020 cm^{-1}. The -C-N stretching vibration of PANI was observed clearly at 1300 cm^{-1}. The main characteristic peaks at 1560 and 1480 cm^{-1} are ascribed to the stretching vibrations of the -C=N quinonoid and the -C=C benzenoid rings of PANI doped with H_2SO_4, respectively [25]. Dipping the emeraldine salt of PANI with ammonium hydroxide yields the dedoped form of PANI, whose two main characteristic peaks (1560 and 1480 cm^{-1}) were shifted to 1590 and 1500 cm^{-1} (curve b), respectively. After the dedoped form of PANI was redoped by PAMA, the two main characteristic peaks were shifted to 1577 and 1494 cm^{-1} (curve c), respectively. The characteristic -C=O group of PANI-PAMA was observed at 1710 cm^{-1}. This indicates that PANI can be doped with PAMA (PANI-PAMA) via a simple doping-dedoping-redoping technique.

3.2. XPS analysis of PANI and PANI-PAMA

XPS is a trustful method for the element analysis. The relative concentrations of C, N, S, and O in PANI and PANI-PAMA are listed in Table 1. The evidence for the successful formation of PANI-PAMA can be observed from the absence of S_{2p} signal and the presence of strong the O_{1s} signal, which can be attributed to that the -CO_2H group in PAMA is incorporated in PANI. The C/N ratio for PANI backbone is close to 6. However, the C/N ratio for PANI-PAMA (C/N=11.6) is higher than 6 due to the existence of PAMA. XPS study was employed to analyze the binding energy related to N_{1s} core-level spectra of PANI, PANI-Pt, PANI-PAMA, and PANI-PAMA-Pt. The N_{1s} core level spectrum of PANI and PANI-Pt on ITO is shown in curve I-II of Fig. 2a. The two curves show significant differences at about 399.8 and 400.3 eV, which are PANI and PANI-Pt, respectively. Deposited Pt particle may have polarization influence on the N_{1s} orbital in PANI structure and this could change the energy level for the PANI-Pt [18]. In contrast, the N_{1s} core level spectrum of PANI-PAMA and PANI-PAMA-Pt (curve III-IV) shows small differences of peak in binding energy due to the presence of PAMA in PANI matrix. The Pt core-level spectra of PANI-Pt and PANI-PAMA-Pt are shown in Fig. 2b. The intensive Pt_{4f} binding energy peaks appeared at 71.3 and 74.7 eV is the significance of metallic Pt [26]. Therefore Pt particles were found to be zero oxidation state in the deposition of Pt on PANI-PAMA electrode. The comparison of Pt_{4f} core-level spectra reveals that the spectra for PANI-Pt and PANI-PAMA-Pt are virtually identical. Hence, the prescribed experimental conditions are highly favored for the formation of Pt particles in PANI-PAMA matrix by electrochemical deposition process.

Table 1. Surface elements (XPS) for PANI and PANI-PAMA

Electrode	C_{1s} (%)	N_{1s} (%)	S_{2P} (%)	O_{1s} (%)
PANI	64.0	10.6	4.1	21.3
PANI-PAMA	61.3	5.3	—	33.3

3.3. Electrodeposition of Pt into PANI and PANI-PAMA

Pt particles were incorporated into PANI and PANI-PAMA films by electrochemical deposition at a constant potential of -0.2 V (vs. Ag/AgCl) with a charge of 0.15 C. Fig. 3a-d show the scanning electron microscopy (SEM) analysis results of surface morphology of PANI, PANI-PAMA, PANI-Pt,

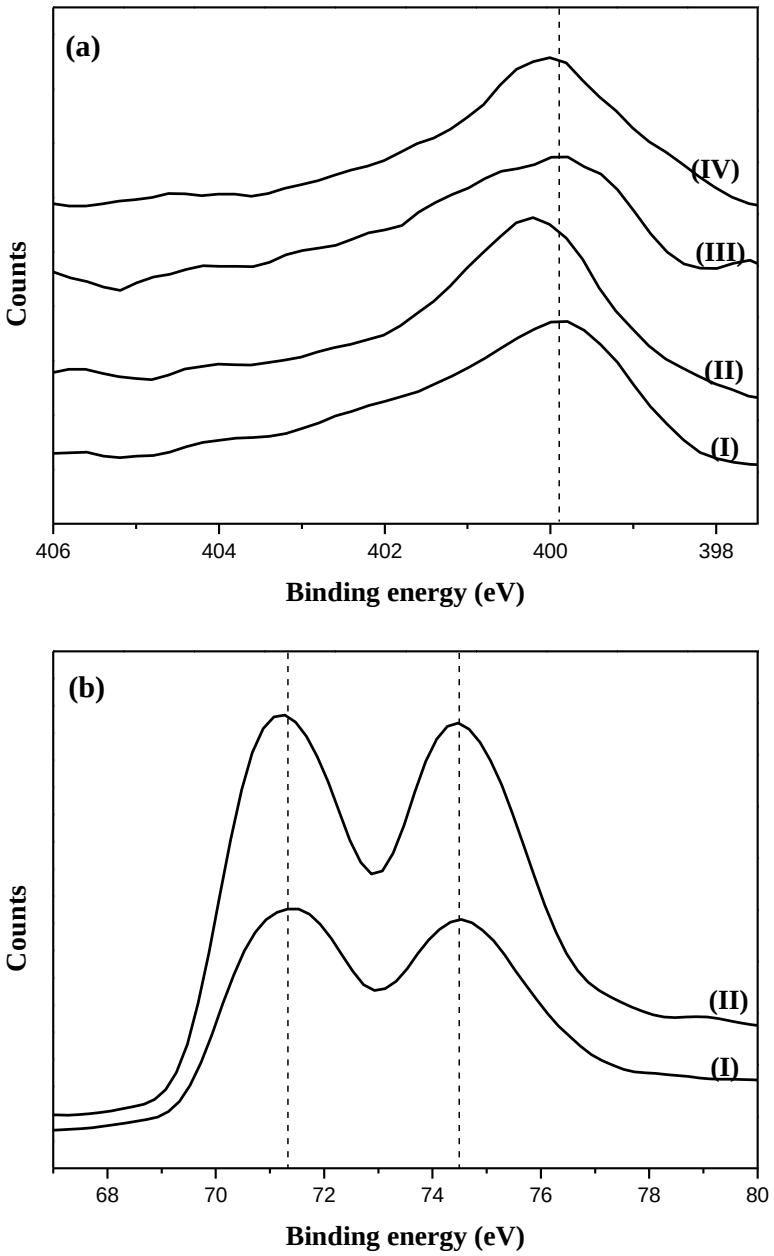

Figure 2. (a) XPS spectra of the N_{1s} core-level of (I) PANI, (II) PANI-Pt, (III) PANI-PAMA, and (IV) PANI-PAMA-Pt. (b) XPS spectra of the Pt_{4f} core-level of (I) PANI-Pt and (II) PANI-PAMA-Pt.

and PANI-PAMA-Pt electrodes; Pt particle mapping analysis results for PANI-Pt and PANI-PAMA-Pt are shown in the inset. The nanowire morphology of PANI and PANI-PAMA films can be clearly seen

in Fig. 3a-b. The PANI nanowires were found to have an average diameter of 40-60 nm. PANI-PAMA nanowires had a much larger diameter (50-70 nm) with a smooth surface due to the influence of PAMA molecules. It is to be noted that the incorporation of PAMA into PANI does not significantly change the nanowire morphology. We believe that Pt particles were incorporated into the PANI and PANI-PAMA nanowire network structures. Pt particles cannot be clearly seen on PANI-Pt and PANI-PAMA-Pt composite electrodes (Fig. 3c-d) from SEM images. Hence, particle mapping analysis was conducted to examine the surface morphology. The insets in Fig. 3c-d show EDS results of Pt in PANI and PANI-PAMA electrodes. The bright spots indicate the existence of platinum in PANI and PANI-PAMA.

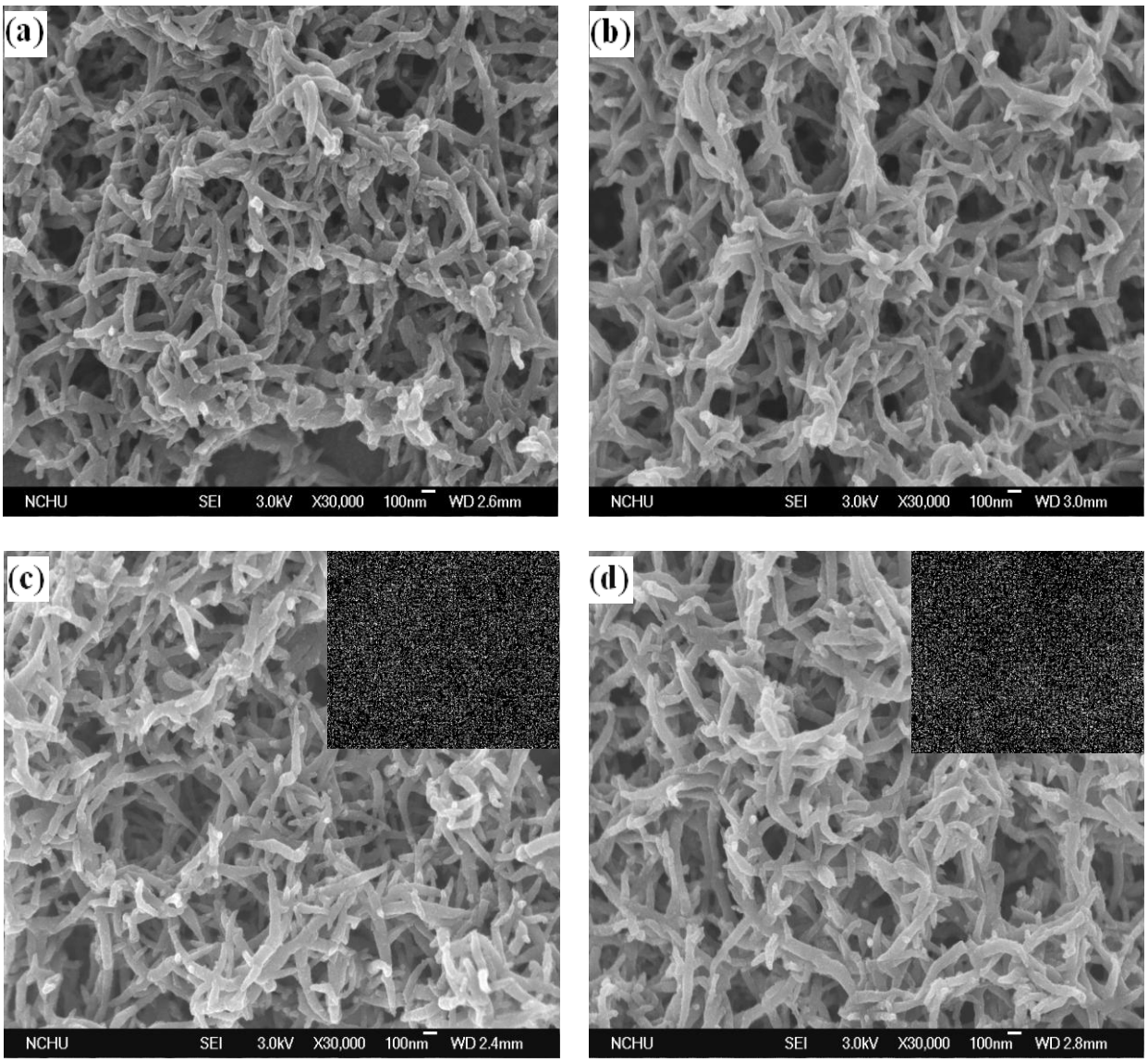

Figure 3. SEM images of (a) PANI, (b) PANI-PAMA, (c) PANI-Pt, and (d) PANI-PAMA-Pt. Insets in (c) and (d) show X-ray maps (bright spots indicate Pt).

The incorporation of Pt into PANI and PANI-PAMA films was examined by the depth profile of Pt particles obtained from Auger electron spectroscopy (AES) (Fig. 4). There is a definite difference in the distribution of particles in PANI-Pt and PANI-PAMA-Pt electrodes. The depth profile of Pt in PANI matrix (curve a) shows an increase in the intensity of Pt to a maximum at 27 min and then a decrease to a shoulder at about 35 min. The curve then decreases sharply at about 37 min. In contrast to the Pt in the PANI-Pt electrode, Pt in the PANI-PAMA matrix (curve b) shows a slow increase in the intensity of Pt with increasing time. Consequently, Pt particles in the PANI-PAMA matrix exhibit a more uniform dispersion than that of those in PANI-Pt. This may be attributed to PANI doped with PAMA forming a spatial network structure (3D-random matrix), CO_2^- groups of PANI-PAMA helping the uptake of Pt^{4+} ions, and a protective layer preventing the aggregation of Pt particles after Pt formation. The homogenous distribution of Pt in the PANI-PAMA spatial network structure may increase the use of Pt for methanol oxidation.

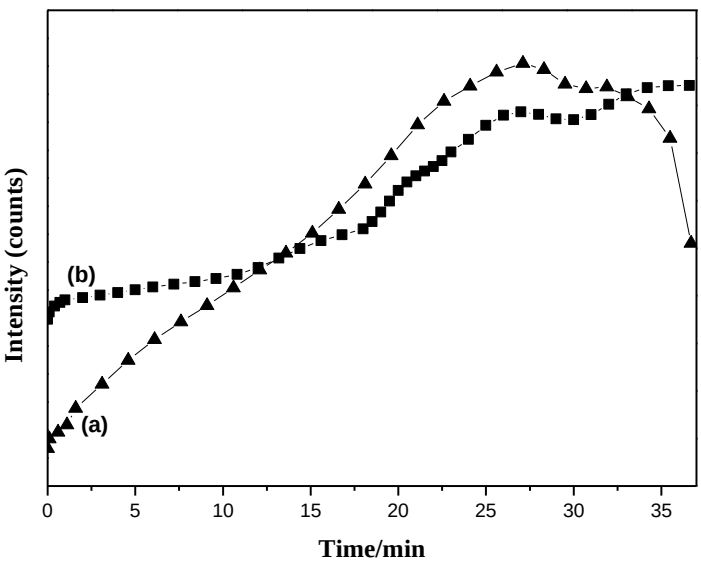

Figure 4. AES depth profiles for Pt within (a) PANI-Pt and (b) PANI-PAMA-Pt.

3.4. Electrocatalytic activity of PANI-PAMA-Pt for methanol oxidation

Cyclic voltammograms (CVs) of PANI-Pt and PANI-PAMA-Pt electrodes recorded at a scan rate of 10 mV/sec in 0.5 M H_2SO_4 are shown in Fig. 5d-e (insets). Three redox pairs can be observed for PANI-PAMA-Pt and PANI-Pt. The A/A' and C/C' redox peaks are respectively attributed to the conversion of leucoemeraldine to emeraldine and the emeraldine to pernigraniline transition for the PANI of PANI-Pt and PANI-PAMA-Pt electrodes. The B/B' peak is associated with the redox reaction of the degradation product containing aromatic quinonoid groups [27]. The PANI-Pt and PANI-PAMA-Pt electrodes present a clear skin texture of hydrogen adsorption/desorption with no sharp peaks in the potential region between -0.2 and +0.0 V vs. Ag/AgCl [28]. There is a difference in the current density of hydrogen absorption between PANI-Pt and PANI-PAMA-Pt electrodes. It is known

that the integrated intensity of hydrogen absorption represents the number of Pt sites that are available for hydrogen adsorption and desorption [29,30]. To calculate the charge required for hydrogen absorption on the electrode surfaces, we assumed that the double-layer charging current is constant over the whole potential range. The charge required for hydrogen absorption on the PANI-PAMA-Pt surface is 3.74 mC/cm^2, which is 1.4 times larger than that required for hydrogen absorption on the PANI-Pt surface (2.72 mC/cm^2) (Table 2). This reveals that PANI-PAMA-Pt has a higher Pt surface area than that of PANI-Pt, which is attributed to the homogeneous dispersion of Pt in the PANI-PAMA spatial network structure. From Fig. 3 (inset) and Fig. 4, the EDS and AES results indicate that the Pt particles are uniformly dispersed in the PANI-PAMA nanowire matrix.

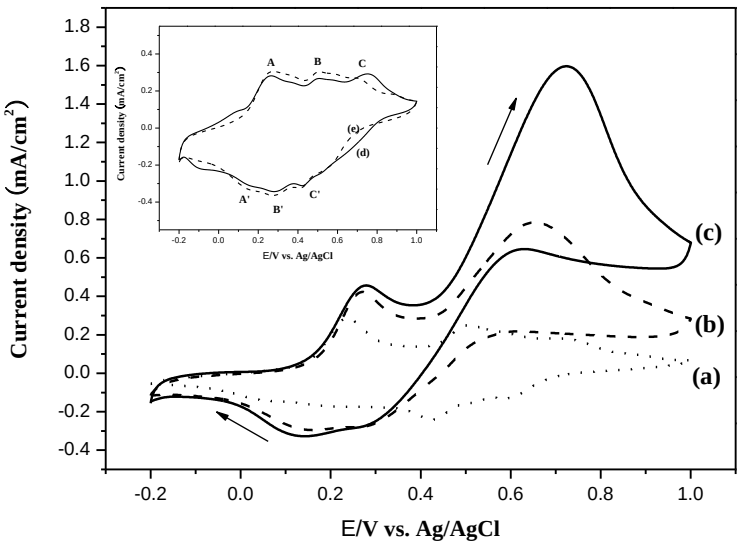

Figure 5. Cyclic voltammograms of (a) PANI, (b) PANI-Pt, and (c) PANI-PAMA-Pt in 0.1 M CH_3OH + 0.5 M H_2SO_4 solution obtained at a scanning rate of 10 mV/sec. Insets: cyclic voltammograms of (d) PANI-PAMA-Pt and (e) PANI-Pt in 0.5 M H_2SO_4 solution obtained at a scanning rate of 10 mV/sec.

CVs are convenient and useful tools for investigating the electrocatalytic activity of test electrodes for methanol oxidation. Fig. 5a-c show the CVs of PANI, PANI-Pt, and PANI-PAMA-Pt composite electrodes in 0.5 M H_2SO_4 solution containing 0.1 M methanol obtained at a scan rate of 10 mV/sec, respectively. The onset potential value of methanol oxidation occurs at about 0.42 and 0.40 V for the electrodes of PANI-Pt and PANI-PAMA-Pt, respectively, indicating that PANI-PAMA-Pt has superior electrocatalytic performance for methanol oxidation. The CVs of the PANI electrode (curve a) show that there is no characteristic methanol oxidation peak at 0.70 V, indicating that only PANI is electrocatalytically inactive toward methanol oxidation. Comparing the CV results of PANI-Pt and PANI-PAMA-Pt electrodes, a significantly higher oxidation current toward methanol oxidation can be observed for the PANI-PAMA-Pt electrode. For instance, maximum anodic peak current densities (Ia in Table 2) of 1.60 mA/cm^2 and 0.78 mA/cm^2 can be observed for PANI-PAMA-Pt and PANI-Pt electrodes at about 0.70 V, respectively.

Table 2. Cyclic voltammetric data for PANI-Pt and PANI-PAMA-Pt electrodes

Electrode	Charge of H_2 adsorption (mC/cm^2)	Methanol oxidation	
		Onset (V)	Ia (mA/cm^2)
PANI-Pt	2.72	0.42	0.78
PANI-PAMA-Pt	3.74	0.40	1.60

A high surface area for Pt particles is anticipated due to the uniform distribution of Pt particles into PANI doped with PAMA can twist up to form a spatial 3D-dimensional matrix. The $-CO_2H$ groups in PANI-PAMA may act as a stabilizer for Pt particles, preventing their aggregation. The PANI-PAMA matrix acts as a good bed for the deposition of Pt particles, and increases the density of the active sites on the electrode surface. The enhanced electrocatalytic activities at the conducting polymer doped with a polymer acid and Pt composites can be attributed to the uniform distribution of particles in the 3D matrix. The above view is supported by previous reports [31,32]. Dalmia *et al.* [31] demonstrated the feasibility of synthesizing nanometer-sized Pt colloids using a negatively charged polymer, poly(N-sulfonatopropyl p-benzamide). Ahmadi *et al.* [32] reported the synthesis of nanometer-sized Pt colloids using polyacrylic acid and investigated the effect of polymer concentration on the shape of Pt particles. Accordingly, Pt in PANI-PAMA significantly improves catalytic activity.

3.5. Chronopotentiometric study of PANI-PAMA-Pt electrode

A chronopotentiometric study was carried out to investigate the anti-poisoning abilities of catalysts toward methanol oxidation [33,34]. For the two catalysts, Fig. 6 shows that the electrode potential increases gradually for several minutes and then jumps to a higher value. This occurs because in the chronopotentiometric experiment, CO accumulates on the surface of Pt particles during the methanol oxidation process and reduces the electrocatalytic activity of catalysts [34]. When the electrocatalysts are greatly poisoned, the methanol oxidation reaction stops.

The time (T) at which the electrode potential jumps to a higher value is introduced to determine the anti-poisoning ability of a catalyst. The T value of PANI-PAMA-Pt (T=12 min) is higher than that (T= 7 min) of the PANI-Pt electrode. These results show that the PANI-PAMA-Pt catalyst has better anti-poisoning ability, which is important for fuel cell operation at conditions similar to those used here. The incorporation of PAMA into PANI may influence the formation of strongly absorbed poisonous species on the surface of Pt particles.

3.6. Electrochemical impedance spectroscopy measurements

Electrochemical impedance spectroscopy (EIS) was used to determine the charge-transfer resistance for PANI-Pt and PANI-PAMA-Pt toward methanol oxidation [35]. Fig. 7 shows the Nyquist plots obtained in 0.1 M CH_3OH + 0.5 M H_2SO_4 solution at an applied potential of 0.40 V vs. Ag/AgCl using an AC amplitude of 10.0 mV for PANI-Pt and PANI-PAMA-Pt electrodes. At a potential of 0.40

V vs. Ag/AgCl, CO absorbed into the surface of Pt particles during the methanol oxidation process. The incorporation of PAMA into PANI may hinder the formation of strongly absorbed poisonous species on the surface of Pt particles. To interpret the impedance results, the equivalent circuit was used to fit the EIS data in Fig. 7 (inset). In this $R_s(R_{ct}CPE)$ circuit, R_s represents ohmic resistance of the solution, R_{ct} is the charge-transfer resistance, and CPE is the constant phase element. The parallel combination of R_{ct} and CPE leads to a depressed semicircle in the corresponding Nyquist impedance plot.

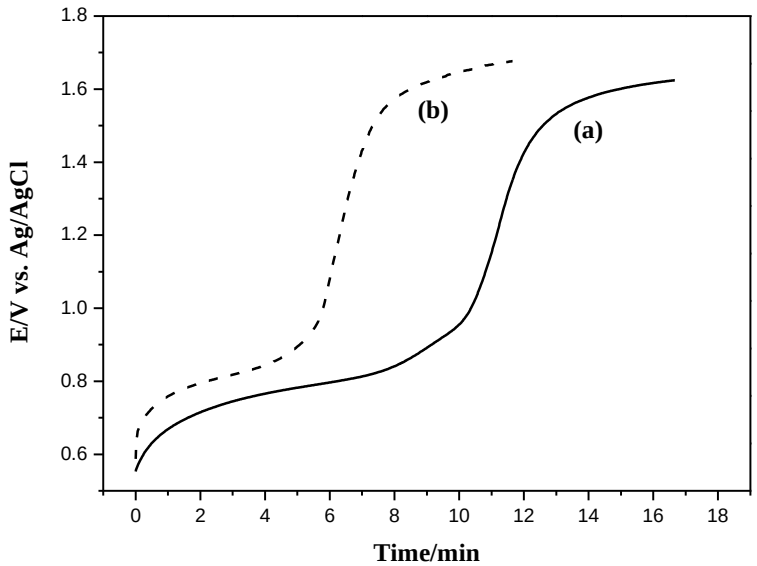

Figure 6. Chronopotentiometric curves of (a) PANI-PAMA-Pt and (b) PANI-Pt in 0.1 M CH_3OH + 0.5 M H_2SO_4 solution obtained at a constant current of 0.08 mA/cm^2.

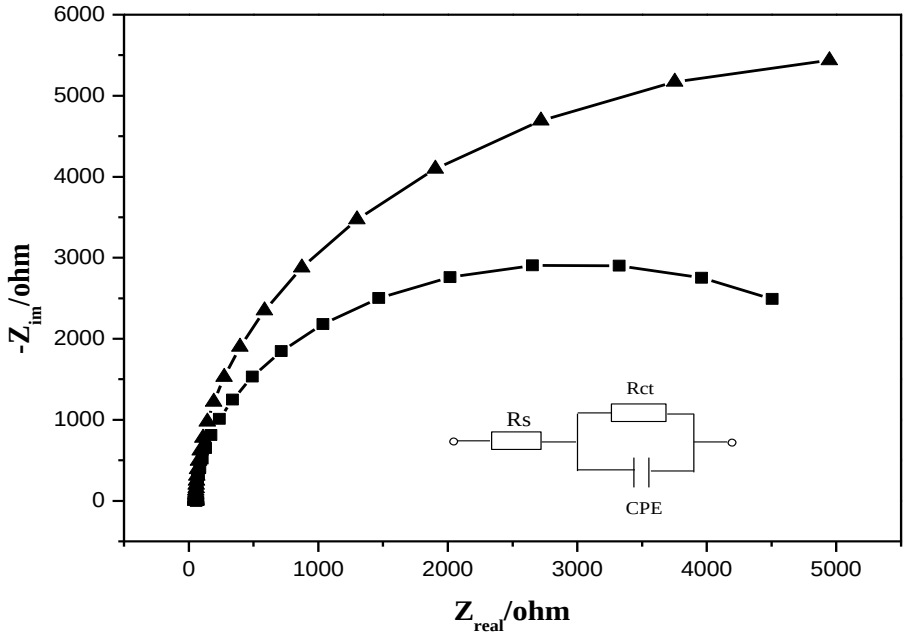

Figure 7. Nyquist plots for PANI-PAMA-Pt (■) and PANI-Pt (▲) electrodes in 0.1 M CH_3OH + 0.5 M H_2SO_4 solution obtained at an applied potential of 0.40 V vs. Ag/AgCl using an AC amplitude of 10.0 mV. The equivalent circuit was used to fit the impedance spectra (inset).

According to experiment data based on equivalent circuits, it is clear that the charge-transfer resistance (R_{ct} = 5.8 kΩ) for PANI-PAMA-Pt is lower than that for PANI-Pt (R_{ct} = 10.9 kΩ) due to the presence of PAMA in the PANI matrix. This means that the Pt particles inside the PANI-PAMA matrix may lead to a faster charge transfer at the PANI-PAMA-Pt film/solution interface compared to that at the PANI-Pt film/solution interface. The incorporation of PAMA into PANI may hinder the formation of strongly absorbed poisonous species.

4. CONCLUSIONS

PANI-PAMA nanowires can be synthesized via a doping-dedoping-redoping method. Pt particles were successfully embedded into the PANI-PAMA nanowire network structure to form a PANI-PAMA-Pt composite electrode. The existence of $-CO_2H$ in the PANI-PAMA spatial structure may stabilized Pt^{4+} ions in the polymer matrix, causing a homogenous distribution of Pt in PANI-PAMA. The PANI-PAMA-Pt electrode exhibits a higher current density and lower onset potential toward methanol oxidation compared to those for PANI-Pt. The composite PANI-PAMA-Pt-based electrode is thus a promising material as a catalyst for methanol oxidation. The enhanced electrocatalytic activity of Pt in PANI-PAMA decreases the use of Pt content in direct-methanol fuel cell applications.

ACKNOWLEDGEMENTS
The financial support of this work by the National Science Council of Taiwan under NSC 99-2218-E-151-003 and KUAS-99-SB-002 are gratefully acknowledged.

References

1. A.S. Aricò, S. Srinivasan, V. Antonucci, *Fuel Cells*, 1 (2001) 13.
2. J.A. Kumar, P. Kalyani, R. Saravanan, *Int. J. Electrochem. Sci.*, 3 (2008) 961.
3. M. Brandalise, M.M. Tusi, R.M.S. Rodrigues, E.V. Spinace, A.O. Neto, *Int. J. Electrochem. Sci.*, 5 (2010) 1879.
4. Y.I. Kim, D. Soundararajan, C.W. Park, S.H. Kim, J.H. Park, J.M. Ko, *Int. J. Electrochem. Sci.*, 4 (2009) 1548.
5. C.M. Bautista-Rodriguez, A. Rosas-Paleta, J.A. Rivera-Marquez, O. Solorza-Feria, *Int. J. Electrochem. Sci.*, 4 (2009) 60.
6. A.O. Neto, R.W.R. Verjulio-Silva, M. Linardi, E.V. Spinace, *Int. J. Electrochem. Sci.*, 4 (2009) 954.
7. J. Parrondo, R. Santhanam, F. Mijangos, B. Rambabu, *Int. J. Electrochem. Sci.*, 5 (2010) 1342.
8. B. Krishnamurthy, S. Deepalochani, *Int. J. Electrochem. Sci.*, 4 (2009) 386.
9. M. Brandalise, M.M. Tusi, R.M. Piasentin, M. Linardi, E.V. Spinace, A.O. Neto, *Int. J. Electrochem. Sci.*, 5 (2010) 39.
10. W. Vielstich, A. Lamm, H.A. Gasteiger, *Handbook of Fuel Cells-Fundamentals, Technology and Applications:* Rotating thin film method for supported catalysis, John Wiley & Sons, New York, 2003, Chapter 22 p. 316.
11. Y.X. Chen, A. Miki, S. Ye, H. Sakai, M. Osawa, *J. Am. Chem. Soc.*, 125 (2003) 3680.

12. R. Baron, F.W. Campbell, I. Streeter, L. Xiao and R.G. Compton, *Int. J. Electrochem. Sci.*, 3 (2008) 556.
13. R. Dillon, S. Srinivasan, A. S. Aricò, V. Antonucci, *J. Power Sources*, 127 (2004) 112.
14. H.J. Wang, H. Yu, F. Peng, P. Lv, *Electrochem. Commun.*, 8 (2006) 499.
15. X.J. Feng , Y.L. Shi, Z.A. Hu, *Int. J. Electrochem. Sci.*, 5 (2010) 489.
16. D. Profeti, P. Olivi, *Electrochim. Acta*, 49 (2004) 4979.
17. J. Li, X. Lin, *J. Electrochem. Soc.*, 154 (2007) B1074.
18. F.J. Liu, L.M. Huang, T.C. Wen, K.C. Yin, J.S. Hung, A. Gopalan, *Polymer Composites*, (2007) 650.
19. F. Xie, Z. Tian, H. Meng, P.K. Shen, *J. Power Sources*, 141 (2005) 211.
20. T.K. Chang, T.C. Wen, *Synth. Met.*, 158 (2008) 364.
21. L.M. Huang, W.R. Tang, T.C. Wen, *J. Power Sources*, 164 (2007) 519.
22. C.W. Kuo, L.M. Huang, T.C. Wen, A. Gopalan, *J. Power Sources*, 160 (2006) 65.
23. T.C. Wang, M.F. Rubner, R.E. Cohen, *Langmuir*, 18 (2002) 3370.
24. F.J. Liu, L.M. Huang, T.C. Wen, C.F. Li, S.L. Huang, A. Gopalan, *Synth. Met.*, 158 (2008) 767.
25. C.W. Kuo, T.C. Wen, *European Polymer Journal*, 44 (2008) 3393.
26. L. Li, H.X. Wang, B.Q. Xu, J.L. Li, T.H. Lu. Z.Q. Mao, *Acta Chimica Sinica*, 61 (2003) 818.
27. S.S. Chen, T.C. Wen, A. Gopalan, *Synth. Met.*, 132 (2003) 133.
28. C. Sivakumar, *Electrochim. Acta*, 52 (2007) 4182.
29. T. J. Schmidt, H. A. Gasteiger, G. D. Stab, P. M. Urban, D. M. Kolb, R. J. Behm, *J. Electrochem. Soc.*, 145 (1998) 2354.
30. A.Chen, D.J.L. Russa, B. Miller, *Langmuir*, 20 (2004) 9695.
31. Dalmia, C.L. Lineken, R.F. Savinell, *J. Colloid & Interface.*, 205 (1998) 535.
32. T.S. Ahmadi, Z.L. Wang, T.C. Green, A. Henglein, M.A. Elsayed, *Science*, 272 (1996) 1924.
33. M. Krausa, W. Vielstich, *J. Electroanal. Chem.*, 399 (1995) 7.
34. J. Chen, M. Wang, B. Liu, Z. Fan, K.Cui,Y. Kuang, *J. Phys. Chem.*, B 110 (2006) 11775.
35. C.W. Kuo, C. Sivakumar, T.C. Wen, *J. Power Sources*, 185 (2008) 807.

© 2011 by ESG (www.electrochemsci.org)